Necrotizing Soft Tissue Infection Staphylococcus aureus but not S. pyogenes Isolates Display High Rates of Internalization and Cytotoxicity Toward Human Myoblasts

Jessica Baude, Sylvère Bastien, Yves Gillet, Pascal Leblanc, Andreas Itzek, Anne Tristan, Michèle Bes, Stéphanie Duguez, Karen Moreau, Binh An Diep, et al.

▶ **To cite this version:**

Jessica Baude, Sylvère Bastien, Yves Gillet, Pascal Leblanc, Andreas Itzek, et al.. Necrotizing Soft Tissue Infection Staphylococcus aureus but not S. pyogenes Isolates Display High Rates of Internalization and Cytotoxicity Toward Human Myoblasts. Journal of Infectious Diseases, 2019, 220 (4), pp.710-719. 10.1093/infdis/jiz167 . hal-02323758

HAL Id: hal-02323758
https://hal.science/hal-02323758v1

Submitted on 10 Jan 2025

HAL is a multi-disciplinary open access archive for the deposit and dissemination of scientific research documents, whether they are published or not. The documents may come from teaching and research institutions in France or abroad, or from public or private research centers.

L'archive ouverte pluridisciplinaire **HAL**, est destinée au dépôt et à la diffusion de documents scientifiques de niveau recherche, publiés ou non, émanant des établissements d'enseignement et de recherche français ou étrangers, des laboratoires publics ou privés.

bioRxiv preprint doi: https://doi.org/10.1101/530493; this version posted January 28, 2019. The copyright holder for this preprint (which was not certified by peer review) is the author/funder, who has granted bioRxiv a license to display the preprint in perpetuity. It is made available under aCC-BY-NC-ND 4.0 International license.

Necrotizing Soft Tissue Infections *Staphylococcus aureus* - but not *Streptococcus pyogenes*- isolates display high rate of internalization and cytotoxicity toward human myoblasts

Jessica Baude[1], Sylvère Bastien[1], Yves Gillet[1,2], Pascal Leblanc[3], Andreas Itzek[4], Anne Tristan[1,2], Michèle Bes[1,2], Stephanie Duguez[5], Karen Moreau[1], Binh An Diep[7], Anna Norrby-Teglund[8], Thomas Henry[1], François Vandenesch[1,2], and INFECT Study Group.

1 CIRI, Centre International de Recherche en Infectiologie, Université de Lyon; Inserm U1111; Ecole Normale Supérieure de Lyon; Université Lyon 1 ; CNRS, UMR5308; Hospices Civils de Lyon ; Lyon, France.

2 Centre National de Référence des Staphylocoques, Institut des Agents Infectieux, Hospices Civils de Lyon, Lyon, France

3 NeuroMyoGene Institute, Université de Lyon, CNRS UMR5310, INSERM U1217, Lyon, France

4 Helmholtz-Zentrum für Infektionsforschung GmbH | Inhoffenstraße 7 | 38124 Braunschweig

5 Northern Ireland Center for Stratified Medicine, Biomedical Sciences Research Institute, Londonderry, UK

6 Centre de biotechnologie cellulaire et Biothèque, Groupe Hospitalier Est, Hospices Civils de Lyon, 69677 Bron, France

7 Division of HIV, Infectious Diseases, and Global Medicine, Department of Medicine, University of California, San Francisco, California, USA

8 Center for Infectious Medicine, Karolinska Institutet, Karolinska University Hospital | Alfred Nobels Allé 8 | 141 52 Huddinge, Sweden

jessica.baude@univ-lyon1.fr

bioRxiv preprint doi: https://doi.org/10.1101/530493; this version posted January 28, 2019. The copyright holder for this preprint (which was not certified by peer review) is the author/funder, who has granted bioRxiv a license to display the preprint in perpetuity. It is made available under aCC-BY-NC-ND 4.0 International license.

29 sylvere.bastien@inserm.fr

30 yves.gillet@chu-lyon.fr

31 pascal.leblanc@univ-lyon1.fr

32 andreas.itzek@live.de

33 anne.tristan@chu-lyon.fr

34 michele.bes@chu-lyon.fr

35 s.duguez@ulster.ac.uk

36 karen.moreau@univ-lyon1.fr

37 binh.diep@ucsf.edu

38 anna.norrby-teglund@ki.se

39 thomas.henry@inserm.fr

40 francois.vandenesch@univ-lyon1.fr

41

42 Corresponding author: francois.vandenesch@univ-lyon1.fr

43

bioRxiv preprint doi: https://doi.org/10.1101/530493; this version posted January 28, 2019. The copyright holder for this preprint (which was not certified by peer review) is the author/funder, who has granted bioRxiv a license to display the preprint in perpetuity. It is made available under aCC-BY-NC-ND 4.0 International license.

Abstract (250 words)

Necrotizing Soft Tissue Infections (NSTIs), often reaching the deep fascia and muscle, are mainly caused by group A *Streptococcus* (GAS) and to a lesser extent by *Staphylococcus aureus* (SA). Conversely SA is a leading etiologic agent of pyomyositis suggesting that SA could have a specific tropism for the muscle. To assess the pathogenicity of these two bacterial species for muscles cells in comparison to keratinocytes, adhesion and invasion of NSTI-GAS and NSTI-SA were assessed on these cells. Bloodstream infections (BSI) SA isolates and non-invasive coagulase negative Staphylococci (CNS) isolates were used as controls.

SA isolates from NSTI and from BSI exhibited stronger internalization into human keratinocytes and myoblasts than CNS or NSTI-GAS. While the median level of SA internalization culminated at 2% in human keratinocytes, it reached over 30% in human myoblasts due to a higher percentage of infected myoblasts (>11%) as compared to keratinocytes (<3%) assessed by transmission electron microscopy. Higher cytotoxicity for myoblasts of NSTI-SA as compared to BSI-SA, was attributed to higher levels of *psm*α and *RNAIII* transcripts in NSTI group as compared to hematogenous group. However, the two groups were not discriminated at the genomic level. The cellular basis of high internalization rate in myoblasts was attributed to higher expression of α5β1 integrin in myoblasts as compared to keratinocytes. Major contribution of FnbpAB-integrin α5β1 pathway to internalization was confirmed by isogenic mutants.

bioRxiv preprint doi: https://doi.org/10.1101/530493; this version posted January 28, 2019. The copyright holder for this preprint (which was not certified by peer review) is the author/funder, who has granted bioRxiv a license to display the preprint in perpetuity. It is made available under aCC-BY-NC-ND 4.0 International license.

Our findings suggest the contribution of NSTI-SA severity by its unique propensity to invade and kill myoblasts, a property not shared by NSTI-GAS.

Importance (150 word)

Necrotizing Soft Tissue Infection (NSTI) is a severe infection caused mainly by group A *Streptococcus* (GAS) and occasionally by *S. aureus* (SA); the latter being more often associated with pyomyositis. NSTIs frequently involve the deep fascia and may provoke muscle necrosis. The goal of this study was to determine the tropism and pathogenicity of these two bacterial species for muscle cells. The results revealed a high tropism of SA for myoblasts and myotubes followed by cytotoxicity as opposed to GAS that did not invade these cells. This study uncover a novel mechanism of SA contribution to NSTI with a direct muscle involvement, while in GAS NSTI this is likely indirect, for instance, secondary to vascular occlusion.

bioRxiv preprint doi: https://doi.org/10.1101/530493; this version posted January 28, 2019. The copyright holder for this preprint (which was not certified by peer review) is the author/funder, who has granted bioRxiv a license to display the preprint in perpetuity. It is made available under aCC-BY-NC-ND 4.0 International license.

Introduction

Necrotizing fasciitis and other necrotizing soft tissue infections (NSTIs) are the most extreme development of skin and soft tissue infections, requiring intensive care and surgical removal of necrotic tissues. NSTI encompass various clinical entities (1, 2). They are characterized anatomically by necrotic infections beyond the subcutaneous tissue and the superficial fascia, often involving the deep fascia and sometimes associated with myonecrosis (2). Based on the polymicrobial or monomicrobial character of the infection, NSTIs are classified as type I and type II, respectively. Type I is a polymicrobial infection involving aerobic and anaerobic organisms and, depending of the study, is either less or equally prevalent to type II (1). Type II is a monomicrobial infection caused by group A Streptococcus (GAS) and to a lesser extent by *Staphylococcus aureus* (SA), notably methicilin-resistant *S. aureus* (MRSA) (3). Although SA is a common cause of superficial SSTI and cellulitis (4), the exact prevalence of SA in NSTI is difficult to assess, principally because of the lack of prospective controlled population-based studies. Myositis has been reported as “an unexpected finding” in SA NSTI cases (3) and SA is typically an agent of pyomyositis, notably in tropical countries (5–8). Altogether, these epidemiological reports suggest a particular tropism and pathogenesis of SA for the skeletal muscles. The aim of the present study was to investigate and compare the invasiveness of muscle cells by SA and GAS as the two major species responsible for type II NSTI. We showed that SA displays a unique

bioRxiv preprint doi: https://doi.org/10.1101/530493; this version posted January 28, 2019. The copyright holder for this preprint (which was not certified by peer review) is the author/funder, who has granted bioRxiv a license to display the preprint in perpetuity. It is made available under aCC-BY-NC-ND 4.0 International license.

104 propensity to invade muscle cells principally via the FnbpAB-integrin α5β1

105 pathway, a property that is not seen in GAS from NSTI patients.

bioRxiv preprint doi: https://doi.org/10.1101/530493; this version posted January 28, 2019. The copyright holder for this preprint (which was not certified by peer review) is the author/funder, who has granted bioRxiv a license to display the preprint in perpetuity. It is made available under aCC-BY-NC-ND 4.0 International license.

Results

SA display enhanced internalization rate in myoblasts as compared to other species. The capacity of both SA and GAS isolates to adhere and invade keratinocyte or myoblasts was evaluated using a gentamicin protection assay. NSTI-SA and bloodstream infections (BSI-SA, used as non-NSTI invasive infections controls) exhibited stronger adhesion than non-invasive coagulase negative Staphylococci (CNS) or NSTI-GAS, onto human keratinocytes (Fig 1A). Internalization into keratinocytes was also significantly higher for NSTI-SA, as compared to the other groups, although the frequencies of infected cells were relatively low (mean 2%) (Fig 1B). Adhesion on and internalization into murine and human myoblasts showed contrasting results. While there were no significant differences between NSTI-SA and NSTI-GAS in adhesion on murine and human myoblasts (Fig 2A and 2B), a dramatic difference in internalization rate was observed, reaching 30-40% for SA (NSTI and BSI) and only 1-5% for NSTI-GAS (Fig 2C and 2D). This very high level of internalization into murine and human myoblast is unique to SA and is shared by all SA strains of the present study. To determine if this high internalization level was caused by a higher mean number of infected cells or by a higher mean number of bacteria per cells, transmission electron microscopy (TEM) was performed on human myoblasts and keratinocytes upon infection by one NSTI-SA (INFECT2127) strain and one SA reference strain (SF8300). The results revealed that the mean number of bacteria per infected cells (actually TEM section) was equivalent in myoblast and keratinocytes (average 3-4 bacteria per infected cell) (Table 1).

bioRxiv preprint doi: https://doi.org/10.1101/530493; this version posted January 28, 2019. The copyright holder for this preprint (which was not certified by peer review) is the author/funder, who has granted bioRxiv a license to display the preprint in perpetuity. It is made available under aCC-BY-NC-ND 4.0 International license.

Conversely the percentage of infected cells was significantly higher in human myoblast (14.62 and 11.43% for INFECT2127 and SF8300, respectively) as compared to keratinocytes (2.86 and 1.43% for INFECT2127 and SF8300, respectively), which is in the order of magnitude of the difference in internalization rates between the two cell types as observed by gentamycin protection assay.

The high rate of SA invasion into muscle cells is not an artifact of immaturity. To rule out the possibility that the observed phenotype in myoblasts could be an artifact of immature cells, the same experiments were performed in myoblast-derived myotubes. Maturity of the cells was assessed morphologically and also by the occurrence of contractibility under video microscopy (Movie S1-S2). In these conditions, the level of internalization of NSTI-SA and BSI-SA was 29.7% and 27.5% respectively, and thus not different to that obtained in myoblasts with the same strains (34.8% and 25.7% for NSTI-SA and BSI-SA respectively) (Fig. S1). These data indicate that the high internalization rate of SA is a shared property of the myoblastic lineage.

FnbpAB is the major determinant of SA internalization into myoblast. To determine which *S. aureus* surface proteins are involved in SA internalization within myoblast, mutant strains for the genes encoding the main effectors of SA internalization, namely, FnbpAB, ClfA, Atl, SdrD, Tet38 and Gap (Table S1) (9), excluding those not present in all our SA strains (Eap), were tested. The results

bioRxiv preprint doi: https://doi.org/10.1101/530493; this version posted January 28, 2019. The copyright holder for this preprint (which was not certified by peer review) is the author/funder, who has granted bioRxiv a license to display the preprint in perpetuity. It is made available under aCC-BY-NC-ND 4.0 International license.

152 revealed a major contribution of FnbpAB. Indeed, while the single *fnb*A and B
153 mutants had no significant phenotype, the double mutant delta-*fnb*AB was
154 internalized 1000-fold less (internalization reduced by 99.999%) than the wild
155 type (WT) strain (Fig. 3). The major impact of FnpbAB was confirmed by using
156 another *fnb*AB double mutant in strain 8325-4 (DU5883) (not shown). Other
157 adhesins also contributed to some extent to internalization into myoblast:
158 mutants in *atl, gap, clf*A and *tet*38 were impaired in internalization by 71%,
159 27.4%, 25% and 24.6 %, respectively, as compared to the WT strain. (Fig. 3).
160
161 **Myoblasts express increased level of Integrin α5β1.** To investigate the
162 cellular basis of high internalization rate of SA in myoblasts (ca 30-40%) as
163 compared to keratinocytes (ca 2%), we analyzed the expression of integrin α5β1
164 (the major target of FnbpAB internalization pathway) on human keratinocyte and
165 myoblasts. Flow cytometry analysis by using an anti-α5β1 antibody showed a
166 greater expression of the α5β1 integrin at the surface of myoblasts as compared
167 to keratinocytes (Fig. 4A)**.** Next, the transcription of integrin α5β1 as well as
168 other eukaryotic surface receptors involved in *S. aureus* internalization (9) was
169 evaluated by RT-qPCR in the two cell lines. The integrin α5β1 displayed
170 contrasting results: whilst integrin β1 was expressed at the same level in both
171 cell lines, integrin α5 was expressed three times more in myoblasts. The
172 expression of integrin β1 was at least 20 times higher than integrin α5,
173 implicating integrin α5 as the limiting partner of the heterodimer (Fig. 4B).
174 Altogether, flow cytometry and RT-qPCR results suggest that functional α5β1 is

bioRxiv preprint doi: https://doi.org/10.1101/530493; this version posted January 28, 2019. The copyright holder for this preprint (which was not certified by peer review) is the author/funder, who has granted bioRxiv a license to display the preprint in perpetuity. It is made available under aCC-BY-NC-ND 4.0 International license.

175 expressed at higher level in myoblasts as compared to keratinocytes. Finally,
176 the major role of integrin α5β1 pathway for SA internalization into myoblasts was
177 confirmed by preincubation of cells with anti-α5β1 antibodies before being
178 challenged by SA, which reduced internalization by more than 65% (Fig. S2).
179 In addition, the transcription of all other cellular receptors known to be involved
180 in SA internalization (IntegrinαV, Integrinβ3, Hsc70, Annexin 2, Hsp60, CD36,
181 gp340) (9) was studied. Increased expression tendancy was generally observed
182 in myoblast as compared to keratinocytes (Fig. S3). Altogether, these results
183 strongly suggest that the higher internalization of SA in myoblast compared to
184 keratinocytes is mediated by various pathways with a preeminence of the FnBP-
185 Fibronectin-α5β1 integrin-mediated pathway.
186
187 **Intracellular *RNAIII* and *psm*α transcript levels correlate with cytotoxicity**
188 **of NSTI-SA.** Since the level of internalization in a given cell type does not inform
189 about the fate of internalized bacteria (i.e. dormancy versus cytotoxicity), the
190 toxicity associated with bacterial internalization was estimated at 24h post-
191 infection by the lactate dehydrogenase (LDH) quantification. NSTI-SA and BSI-
192 SA were as cytotoxic as GAS on keratinocytes; of note CNS were significantly
193 less cytotoxic toward this cell line than other bacterial groups. The most
194 noticeable cytotoxic effect of NSTI-SA was observed on murine and human
195 myoblasts as compared to all other groups, namely NSTI-GAS, CNS, and
196 unexpectedly BSI-SA. (Fig. 5). Of note, the culture supernatant from SA and
197 GAS cultures did not produce cytotoxicity on keratinocytes and myoblasts (Fig

bioRxiv preprint doi: https://doi.org/10.1101/530493; this version posted January 28, 2019. The copyright holder for this preprint (which was not certified by peer review) is the author/funder, who has granted bioRxiv a license to display the preprint in perpetuity. It is made available under aCC-BY-NC-ND 4.0 International license.

198 S4), assessing that the observed cytotoxicity was not caused by toxins or other
199 products released by the bacteria. To elucidate the basis of higher cytotoxicity
200 for myoblasts of NSTI-SA as compared to BSI-SA, the level of the major
201 effectors of intracellular *S. aureus* cytotoxicity, namely PSMα, Hla, Ldh and Agr-
202 RNAIII (10, 11) were assessed by RT-qPCR. The levels of *RNAIII* and *psmα*
203 were significantly higher in NSTI-SA strains as compared to BSI-SA in
204 intracellular conditions into human myoblasts (Fig. 6) as well as from planktonic
205 culture (data not shown). In contrast, the level of *hla* and *ldh* transcript were not
206 significantly different between the two groups.
207
208 **Differences in cytoxicity between NSTI-SA and BSI-SA is not resolved at**
209 **the genomic level.**
210 In order to confirm that the differences between NSTI-SA and BSI-SA isolates
211 in *RNAIII* and *psmα* expression were not related to a genomic bias, a genomic
212 analysis was conducted on the 30 *S. aureus* strains. Phylogenetic analysis
213 based on core-genome confirmed that NSTI and hematogenous strains were
214 phylogenetically entangled (Fig. S5). Virulence factor distribution assessed by
215 micro-array or WGS was not contributive to distinguish NSTI-SA from BSI-SA
216 isolates (Table 2). Notably, there was no virulence factors discriminating the two
217 groups. Detailed genomic could not identify discriminant marker between the
218 two groups either considering genomic determinants presence/absence
219 (including ncRNA, virulence genes,…) or single nucleotide polymorphism
220 (SNPs) (Text. S1).

bioRxiv preprint doi: https://doi.org/10.1101/530493; this version posted January 28, 2019. The copyright holder for this preprint (which was not certified by peer review) is the author/funder, who has granted bioRxiv a license to display the preprint in perpetuity. It is made available under aCC-BY-NC-ND 4.0 International license.

Discussion

Necrotizing fasciitis is a rare disease that involves superficial fascia and results in the extensive damage and necrosis of the surrounding tissue including muscle. In the present study we show that SA may contribute to this disease by its unique propensity to invade muscle cells and consequently trigger cell death, a property that is not seen in GAS from NSTI patients. Interestingly, this unique capacity of *S. aureus* to invade myoblast and myotube from both mice and human origin is uncommon, as neither CNS nor GAS did internalize in those cells to such efficiency. Moreover, to our knowledge, there is no other type of eukaryotic cells in which SA internalizes at this level (over 30%), e.g. the level of SA internalization is ca. 17% in human embryonic kidney cells (12), 8% in endothelial cells (12), 2% in human alveolar epithelial cells (A549) (K. Moreau, unpublished data), <1% HELA epithelial cells (13), <1% within osteoblast (14) and <2% in osteoclast (15). We could demonstrate that this high rate of internalization depends on several of the known pathways of *S. aureus* internalization with a preeminence of the FnBP-Fibronectin-α5β1 integrin-mediated pathway. The increased expression at the surface of human myoblasts of α5β1 integrin and other known receptors involved in SA internalization (integrin αV and β3, HSC70, Annexin 2, Hsp60, CD36 and Gp340) is a likely explanation for the high internalization rate of SA within myoblasts as compared to keratinocytes. This model is also consistent with TEM observation of a higher percentage of infected cells as compared to

bioRxiv preprint doi: https://doi.org/10.1101/530493; this version posted January 28, 2019. The copyright holder for this preprint (which was not certified by peer review) is the author/funder, who has granted bioRxiv a license to display the preprint in perpetuity. It is made available under aCC-BY-NC-ND 4.0 International license.

keratinocytes. The direct consequence of this high rate of internalization within myoblast is a higher cytotoxicity to these cells, and not, as observed in other setting a reduced cytotoxicity associated with high internalization rate (11).

Virulence factors that could be associated with NSTI-SA have been largely debated, Panton Valentine Leucocidin being frequently reported in US studies involving community-acquired MRSA USA300 (3). Other cases associated with *tst*- (16) or with *egc*-encoding isolates were reported (17), reminiscent of the involvement of superantigens in severe GAS tissue infections (18). Noticeably, the 9 NSTI-SA strains of the present study were not clonally related; none of these were MRSA and a single one was PVL-positive (Table 2). Their genetic content regarding virulence factors including superantigens was not significantly different from the BSI-SA strains that represent another major invasive disease (Table 2). WGS comparison by multiple approaches could not discriminate the two diseases isolate groups (Text S1). This lack of discrimination might be caused by the small size of the NSTI group leading to insufficient statistical power. However, the observation that BSI-SA were less cytotoxic than NSTI-SA with similar internalization rate (Fig. 5), is in accordance with previous studies showing that skin and soft tissue infection isolates produce more PSMα (as observed in our study with NSTI isolates) than infective endocarditis or hospital-acquired pneumonia isolates (19). This is also reminiscent of previous observation suggesting an association between low-toxicity and bacteraemia (20): It has been hypothesized that such invasive bloodstream infections limit the opportunities for onward transmission, whilst highly toxic strains associated

bioRxiv preprint doi: https://doi.org/10.1101/530493; this version posted January 28, 2019. The copyright holder for this preprint (which was not certified by peer review) is the author/funder, who has granted bioRxiv a license to display the preprint in perpetuity. It is made available under aCC-BY-NC-ND 4.0 International license.

with skin infections could gain an additional between-host fitness advantage, potentially contributing to the maintenance of toxicity at the population level (20). Altogether this analysis reveal that despite similar virulence factor repertoire, NSTI-SA and BSI-SA isolates differ in their phenotypic expression of virulence and may thus be considered as different pathovars.

The respective contribution of GAS and SA to NSTI is a matter of debate. Of note, the four strains of GAS isolated from NSTI patients, despite being isolated from very severe cases of NSTI, did not present a strong invasive capacity for muscle cells *in vitro*. This result is counter-intuitive given the involvement of epidermis, dermis, subcutaneous tissue, fascia, and muscle in GAS-NSTI (1). This suggests that the muscle involvement in GAS NSTI does not result from bacterial invasion of muscle cells whilst it could be the cases for SA-NSTI when muscle involvement occurs as described (3). However, if the muscle destruction seen in GAS-NSTI is not caused by direct intracellular toxicity of GAS, it is likely not caused either by the toxicity of secreted enzymes and toxins for the muscle cells, as culture supernatant neither from GAS nor from SA had any significant toxicity on cultured myoblasts. It is thus more likely that muscle necrosis in GAS-NSTI results from vascular occlusion secondary to platelet-leukocytes aggregation in response to infection of the adjacent anatomical skin and soft tissue structures.

In conclusion, our results uncover new insight into the pathophysiology of GAS and SA-NSTI and provide a new cellular basis for the contribution of *S. aureus*

bioRxiv preprint doi: https://doi.org/10.1101/530493; this version posted January 28, 2019. The copyright holder for this preprint (which was not certified by peer review) is the author/funder, who has granted bioRxiv a license to display the preprint in perpetuity. It is made available under aCC-BY-NC-ND 4.0 International license.

289 to pathogenesis of NSTI and other deep-seated infection involving the muscle.
290 It also sustains the potential synergy of GAS and SA in NSTI, a situation that is
291 not uncommon (2, 21). It advocates for future prospective clinical study
292 systematically depicting the anatomical tissue layers of infection according to
293 the micro-organisms.

bioRxiv preprint doi: https://doi.org/10.1101/530493; this version posted January 28, 2019. The copyright holder for this preprint (which was not certified by peer review) is the author/funder, who has granted bioRxiv a license to display the preprint in perpetuity. It is made available under aCC-BY-NC-ND 4.0 International license.

Material and Methods

Ethics statement

Muscle biopsies for myoblast cell line were obtained from the Bank of Tissues of Research (Myobank BTR, a partner in the EU network EuroBioBank) in accordance with European recommendations and French legislation. Muscle biopsies for experiment in primary myoblast were obtained from NeuroBioTec (Hospices Civils de Lyon, *Centre de Ressources Biologiques*) and declared to the Ministry of Research under the agreement DC 2011-1437 and the number of accession AC 2012-1867.

Bacterial strains

Bacterial isolates are listed in Table 3. They include strains of *S. aureus* (n=4) and *S. pyogenes* (n=4) isolated from patients included in the INFECT (Improving Outcome of Necrotizing Fasciitis: Elucidation of Complex Host and Pathogen Signatures that Dictate Severity of Tissue Infection) cohort which is an international, prospective, multicenter observational research project (Clinical Trials #NCT01790698). In addition, 5 *S. aureus* strains from French NSTI patients spontaneously referred to the French National Reference Laboratory for Staphylococci were included. The diagnosis of NSTI was made by the surgeon during the primary operation. It is based on, but not restricted to, findings of necrosis, dissolved or deliquescent soft tissue, and fascial and muscular affection (22). The invasive non-NSTI SA control strains consisted in

bioRxiv preprint doi: https://doi.org/10.1101/530493; this version posted January 28, 2019. The copyright holder for this preprint (which was not certified by peer review) is the author/funder, who has granted bioRxiv a license to display the preprint in perpetuity. It is made available under aCC-BY-NC-ND 4.0 International license.

317 Bloodstream infection (BSI) strains (12 infective endocarditis, 9 bacteremia
318 without infective endocarditis) collected during a prospective cohort study on *S.*
319 *aureus* bacteremia (VIRSTA) (23). Those strains were chosen in order to
320 genotypically match NSTI strains on the basis of micro-array-deduced clonal
321 complexes (23) confirmed by whole genome sequencing (Illumina MiSeq
322 technology, Illumina, San Diego, USA, with 16-266 x coverage, median 137).
323 Non *aureus*-staphylococci were type strains of the most frequently isolated CNS
324 species. Strains USA300 JE2 and several transposons insertion mutants in
325 genes encoding proteins potentially involved in internalization (*atl*, *clfA*, *sdrD*,
326 *tet38*, *gap*, *strA*, *strB*) were retrieved from the public Nebraska library (24) with
327 substantial help of Ken Bayles. In-frame deletion of the *fnb*A, *fnb*B and double
328 mutant in the SF8300 background were performed as described previously (25,
329 26) using the pKOR1 allelic replacement mutagenesis system and the primers
330 shown in Table S2 in the supplemental material. Laboratory strains and
331 plasmids are listed in Table S1. All strains were cultured in Brain-Heart infusion
332 (BHi Becton Dickinson) broth under agitation (200 rpm) at 37°C.
333
334 **Cells and culture conditions.** The human keratinocytes N/TERT-1 cells (27)
335 were cultured in keratinocyte SFM media (Thermofisher) at 37°C under 5% CO_2
336 atmosphere. The murine myoblast cells C2C12 (28) were cultured in Dulbecco's
337 Modified Eagle's Medium (Thermofisher) supplemented with 20% Fetal Bovine
338 Serum (Gibco) and 1% penicillin/streptomycin. Murine myoblasts were
339 differentiated into myotubes by addition of 2% of horse serum (Sigma) in the

bioRxiv preprint doi: https://doi.org/10.1101/530493; this version posted January 28, 2019. The copyright holder for this preprint (which was not certified by peer review) is the author/funder, who has granted bioRxiv a license to display the preprint in perpetuity. It is made available under aCC-BY-NC-ND 4.0 International license.

medium. The human myoblast line was obtained as follows. Deltoid muscle biopsy from a 71-year-old male was obtained from the Myobank BTR (see ethical above). Muscle stem cells were extracted, sorted and tested for their myogenicity as previously described (29). Cells were then expended in proliferating KMEM medium (1 volume of M199, 4 volumes of Dulbecco's modified Eagle's medium (DMEM), 20% fetal bovine serum (v/v), 25 µg/ml Fetuin, 0.5 ng/ml bFGF, 5 ng/ml EGF, 5 µg/ml Insulin). The lentiviral vector particles were produced by transient transfection of the packaging construct (HIV-1 psPAX2), a minimal genome (HIV-1 pLv-hTERT-CDK4 from CloneSpace LLC ref SKU: CS1031) bearing the expression cassettes encoding the Htert and CDK4 proteins and the puromycin resistance, and the VSV-G-envelope expressing plasmid pMDG2 (DNA ratio 8:8:4 µg) into 293T cells (3.5 x 10^6 cells plated 1 day before transfection in 100-mm dishes) by the calcium phosphate method (30). Viral particles were normalized by an exogenous reverse transcriptase assay and titrated on human primary myoblast cells (31). Transductions of human primary myoblasts were carried out with different MOI in 12 well plates (80,000 cells plated 1 day before) in presence of 6 µg/ml of polybrene overnight in KMEM culture medium as previously described by Thorley (32). One day after transduction, cells were passaged and cultured in presence of puromycin (1 mg/ml) during 3-4 days until the death of non-transduced primary myoblast control cells was completed. Once puromycin selected, transduced myoblasts were cultured in KMEM-D medium (KMEM medium with dexamethasone 0.2 mg/ml) in absence of puromycin. After one

bioRxiv preprint doi: https://doi.org/10.1101/530493; this version posted January 28, 2019. The copyright holder for this preprint (which was not certified by peer review) is the author/funder, who has granted bioRxiv a license to display the preprint in perpetuity. It is made available under aCC-BY-NC-ND 4.0 International license.

363 week of culture in KMEM-D medium, immortalized myoblasts could be cultured
364 for long term.
365
366 **Adhesion, internalization, survival and cytotoxic assays.**
367 The intracellular infection of cells was performed using gentamycin protection
368 assay as described elsewhere with modifications (33). Cells were seeded at
369 80,000 cells/well in 24-well plates and incubated at 37°C with 5% CO_2 for 24 h
370 in culture medium. Bacterial cultures (9h of growth) were washed with PBS and
371 resuspended in antibiotic-free culture medium at a concentration corresponding
372 to a MOI of 10. The MOIs were subsequently confirmed by CFU counting upon
373 agar plate inoculation. Cells were washed twice in PBS to remove antibiotics,
374 and normalized bacterial suspensions were added to the wells. The infected
375 cultures were incubated for 2h at 37°C and then washed with PBS. The cells
376 used to assay invasion were incubated for an additional 1h at 37°C in culture
377 medium containing 200 mg/L gentamicin and 10 mg/L lysostaphin to rapidly kill
378 extracellular but not intracellular bacteria. To assay bacterial persistence, the
379 cultures were further incubated in medium containing 40 mg/L gentamicin and
380 10 mg/L lysostaphin for 24h. These lower concentrations resulted in the killing
381 of bacteria cells released upon host cell lysis, thus preventing infection of new
382 host cells. Cells used to evaluate adhesion (2h post-infection), invasion (3h
383 post-infection) and persistence (24h post-infection) were lysed by osmotic shock
384 in sterile pure water, and extensively pipetted to achieve the full release of
385 bacteria. The bacterial suspension was plated on Trypcase Soy Agar (TSA;

bioRxiv preprint doi: https://doi.org/10.1101/530493; this version posted January 28, 2019. The copyright holder for this preprint (which was not certified by peer review) is the author/funder, who has granted bioRxiv a license to display the preprint in perpetuity. It is made available under aCC-BY-NC-ND 4.0 International license.

bioMérieux, Marcy l'Etoile, France). After 24h of incubation at 37°C, the colonies were enumerated using an EasyCount automated plate reader (AES Chemunex). Infected cell death was quantified by the release of the cytosolic enzyme LDH into the culture supernatant at 24h post-infection using the CytoTox-ONE Homogeneous Membrane Integrity Assay (Promega) according to the manufacturer's instructions. LDH release into the supernatant of infected cells was compared to that of uninfected cells that were either left intact (lower control) or fully lysed by osmotic shock (higher control). The percentage of cytotoxicity was calculated as follows: ((LDH infected cells - LDH lower control)/(LDH higher control - LDH lower control)) x100.

Relative quantification of bacterial RNA by RT-qPCR

Cells lines were infected as described above. After the first antibiotic treatment, cells and bacteria were harvested by trypsin detachment and centrifugation. Pellet was treated with 20 µg lysostaphin (1 mg/ml) and RNA isolation was performed using the RNeasy Plus mini kit (QIAGEN) according to the manufacturer's instructions. The RNA was quantified using a NanoDrop spectrophotometer, and 100 ng of total RNA was reverse transcribed into cDNA using Reverse Transcriptase System (Promega). Two µL of 1/5 diluted cDNA was used as a template for the real-time PCR amplification using PowerUp SYBR® Green Master Mix and a StepOne Plus system (Applied Biosystem) with specific primers shown in Table S2. Genes expression analysis was performed by using ΔCt methods using *hu* gene as an internal standard and confirmed by

bioRxiv preprint doi: https://doi.org/10.1101/530493; this version posted January 28, 2019. The copyright holder for this preprint (which was not certified by peer review) is the author/funder, who has granted bioRxiv a license to display the preprint in perpetuity. It is made available under aCC-BY-NC-ND 4.0 International license.

409 *gyr*B gene.

410

411 **Relative quantification of eukaryotic receptors by RT-qPCR.**

412 Total RNA was isolated from CTi400 and N/TERT-1 cells using RNeasy Plus
413 mini kit (QIAGEN) according to the manufacturer's instructions. Complementary
414 DNA (cDNA) was synthesized from 1 µg of total RNA using random primers and
415 Reverse Transcriptase System (Promega). The cDNA was used as a template
416 for the real-time PCR amplification using PowerUp SYBR® Green Master Mix
417 and a StepOne Plus system (Applied Biosystem) with specific primers shown in
418 Table S2. Genes expression analysis was performed by using ΔCt methods
419 using β-*actin* gene as an internal standard and confirmed by GAPDH.

420

421 **Transmission Electron Microscopy**

422 Infected cells were fixed in glutaraldehyde 2% and washed three times in
423 saccharose 0.4M and sodium cacodylate buffer 0.2M pH 7.4 for 1h at 4°C, and
424 postfixed with 2% OsO4 and Na C-HCl Cacodylate 0.3M pH 7.4 30 minutes at
425 room temperature. Cells were then dehydrated with an increasing ethanol
426 gradient (5 minutes in 30%, 50%, 70%, 95%, and 3 times 10 minutes
427 in absolute ethanol). Impregnation was performed with Epon A (50%) plus
428 Epon B (50%) plus DMP30 (1.7%). Inclusion was obtained by polymerisation at
429 60°C for 72h. Ultrathin sections (approximately 70 nm thick) were cut on a
430 ultracut UC7 (Leica) ultramicrotome, mounted on 200 mesh copper grids coated
431 with 1:1,000 polylisine, stabilized for 1 day at room temperature and, contrasted

bioRxiv preprint doi: https://doi.org/10.1101/530493; this version posted January 28, 2019. The copyright holder for this preprint (which was not certified by peer review) is the author/funder, who has granted bioRxiv a license to display the preprint in perpetuity. It is made available under aCC-BY-NC-ND 4.0 International license.

with uranyl acetate. Sections were examined with a Jeol 1400JEM (Tokyo,Japan) transmission electron microscope equipped with a Orius 600 camera and Digital Micrograph. Cells were visually examined (175 myoblasts, 455 keratinocytes) to assess the number of infected cells and the number of bacteria per infected cells.

Flow cytometry

Cells were trypsinized, washed and suspended in PBS at a concentration of 1.10^6 per ml, and aliquots were incubated with Fc Block (ThermoFisher Scientific 14-9161-71) 20 minutes at 4°C. The primary α5β1 integrin antibody (10 µg/mL) (Merck Millipore MAB1999) was added for 30 minutes at 4°C. Cells were washed, resuspended in PBS before incubation with Alexa Fluor 647 secondary antibody (10 µg for 10^6 cells) (Themofisher Scienfitic A-21236) for 30 minutes at 4°C and then washed 2 times in PBS. Finally, cells were assessed using a BD Accuri-C6 (BD Biosciences, Le pont de Claix, France) flow cytometer.

Statistical analysis

The statistical analyses were performed using GraphPad Prism 6 software. Data from two groups were compared using either Student's 2-tailed t-test for paired samples or Mann Whitney test for unpaired samples. Data from more than two groups were analyzed using multiple pairwise comparisons of the means

bioRxiv preprint doi: https://doi.org/10.1101/530493; this version posted January 28, 2019. The copyright holder for this preprint (which was not certified by peer review) is the author/funder, who has granted bioRxiv a license to display the preprint in perpetuity. It is made available under aCC-BY-NC-ND 4.0 International license.

454 through a one-way ANOVA including post-hoc tests corrected by a Bonferroni
455 method. The significance threshold was set at 0.05 for all tests.
456
457
458 **Acknowledgments**
459 The authors thank Lam Thuy Hoang, Marine Ibranosyan for help in clinical data
460 management, Ken Bayles for help in providing Nebraska library mutants, Paul
461 Verhoven for fruitful discussions, Laurent Schaeffer, Emilie Chopin and Nathalie
462 Streichenberger from NeuroBio Tec-Banques (Hospices Civils de Lyon, France)
463 for sharing expertise on muscle cells, CIQLE for technical assistance for
464 microscopy, Katia Ziadna for all the agar plates and Laurence Cluzeau for
465 excellent technical support. This work was supported by the EU grant INFECT-
466 EU-FP7-HEALTH.

bioRxiv preprint doi: https://doi.org/10.1101/530493; this version posted January 28, 2019. The copyright holder for this preprint (which was not certified by peer review) is the author/funder, who has granted bioRxiv a license to display the preprint in perpetuity. It is made available under aCC-BY-NC-ND 4.0 International license.

Figure legends

Fig. 1. Adhesion and internalization of *Staphylococcus aureus* (SA), coagulase negative *Staphylococcus* (CNS) and group A *Streptococcus* (GAS) to human keratinocytes. (A) Percentages of adhered bacteria were calculated after 2 hours of infection in relation to inoculum of infection. Intracellular bacteria assessed in B were subtracted; (B) Internalization was determined after 2 hours of infection followed by antibiotic treatment to exclude extracellular bacteria. Multiplicity of infection (MOI) = 10. The horizontal lines within each group represent the mean value ± standard deviations of at least three independent experiments per strain. *p<0.05, **p<0.01, *** p<0.001.

Fig. 2. Adhesion and internalization of *Staphylococcus aureus* (SA), coagulase negative *Staphylococcus* (CNS) and group A *Streptococcus* (GAS) to murine and human myoblasts. (A and B) Percentages of adherent bacteria were calculated after 2 hours of infection in relation to inoculum of infection. Intracellular bacteria assessed in C and D were subtracted; (C and D) Internalization was determined after 2 hours of infection followed by antibiotic treatment to exclude extracellular bacteria. Multiplicity of infection (MOI) = 10. The horizontal lines within each group represent the mean value ± standard deviations of at least three independent experiments per strain. *p<0.05, **p<0.01, *** p<0.001, ****p<0,0001.

bioRxiv preprint doi: https://doi.org/10.1101/530493; this version posted January 28, 2019. The copyright holder for this preprint (which was not certified by peer review) is the author/funder, who has granted bioRxiv a license to display the preprint in perpetuity. It is made available under aCC-BY-NC-ND 4.0 International license.

Fig. 3. Internalization of *S. aureus* mutants into human myoblasts. Internalization of the various mutants in genes encoding surface proteins was determined after 2 hours of infection followed by antibiotic treatment to exclude extracellular bacteria. The internalization was normalized to that of wild type strain. Multiplicity of infection (MOI) = 10. All values are means ± standard error of mean of three independents experiments in duplicate for each strain. *p<0.05, **p<0.01, *** p<0.001, ****p<0,0001.

Fig. 4. Expression of α5β1 integrin by human keratinocyte and myoblasts. (A) Cell surface expression of α5β1 integrin assessed by flow cytometry and α5β1 antibody**;** (B) Relative transcript levels of α5, β1 integrin sub-units were determined using quantitative reverse-transcriptase PCR, normalized to the internal *β-actin* standard. All values are means ± standard error of mean of four independents experiments.

Fig. 5. Cytotoxicity of intracellular bacteria at 24h post infection. Cytotoxicity was estimated by quantifying LDH release by infected cells at 24 hours post infection. Multiplicity of infection (MOI) = 10. The percentage of cytotoxicity was calculated as follows: ((LDH infected cells - LDH lower control)/(LDH higher control - LDH lower control)) x100. The horizontal lines within each group represent the mean value ± standard deviations of at least three independent experiments per strain. *p<0.05, **p<0.01, *** p<0.001, ****p<0,0001.

bioRxiv preprint doi: https://doi.org/10.1101/530493; this version posted January 28, 2019. The copyright holder for this preprint (which was not certified by peer review) is the author/funder, who has granted bioRxiv a license to display the preprint in perpetuity. It is made available under aCC-BY-NC-ND 4.0 International license.

513

514 **Fig. 6. Expression of intracellular bacterial mRNA into human myoblasts**
515 **3 hours post infection.** Relative transcript levels were determined using
516 quantitative reverse-transcriptase PCR and expressed as n-fold change to the
517 internal *hu* standard. The horizontal lines within each group represent the mean
518 value ± standard deviations. *p<0.05, **p<0.01.

519

bioRxiv preprint doi: https://doi.org/10.1101/530493; this version posted January 28, 2019. The copyright holder for this preprint (which was not certified by peer review) is the author/funder, who has granted bioRxiv a license to display the preprint in perpetuity. It is made available under aCC-BY-NC-ND 4.0 International license.

520 **Supplemental material**

521

522 **Movie S1-S2. Murine myotubes.** Mature murine myotubes show spontaneous
523 contractions.

524

525 **Fig. S1. Comparison of internalization of *Staphylococcus aureus* into**
526 **murine myotubes and myoblasts.** The murine myoblast cells C2C12 were
527 cultured in Dulbecco's Modified Eagle's Medium (Thermofisher) supplemented
528 with 10% Fetal Bovine Serum (FBS) and 1% penicillin/streptomycin. Myoblasts
529 were differentiated into myotubes by the addition of 2% horse serum in the
530 medium for eight days. Internalization was determined after 2 hours of infection
531 followed by antibiotic treatment to exclude extracellular bacteria. Percentage of
532 numbers of viable bacteria was calculated in relation to infection inoculum.
533 Multiplicity of infection (MOI) = 10. The diagram represents the mean ±
534 standard deviations from three independent experiments of 6 NSTI-SA and 3
535 BSI-SA.

536

537 **Fig. S2. *Staphylococcus aureus* invasion is mediated by the eukaryotic**
538 **fibronectin receptor α5β1 integrin.** Cells preincubated with monoclonal
539 function-blocking antibodies were challenged with *S. aureus* strain
540 RN6390ΔspA (A. Tristan, Y. Benito, R. Montserret, S. Boisset, E. Dusserre, F.
541 Penin, F. Ruggiero, J. Etienne, H. Lortat-Jacob, G. Lina, M. Gabriela Bowden
542 and F. Vandenesch, PLos ONE 4(4): e5042.

bioRxiv preprint doi: https://doi.org/10.1101/530493; this version posted January 28, 2019. The copyright holder for this preprint (which was not certified by peer review) is the author/funder, who has granted bioRxiv a license to display the preprint in perpetuity. It is made available under aCC-BY-NC-ND 4.0 International license.

543 doi:10.1371/journal.pone.0005042). This strain was chosen to avoid possible
544 interference of Fc binding to staphylococcal protein (SpA) present in all *S.*
545 *aureus* strains. Internalization was determined after 2 hours of infection followed
546 by antibiotic treatment to exclude extracellular bacteria. Percentage of numbers
547 of viable bacteria was calculated in relation to infection inoculum. Multiplicity of
548 infection (MOI) = 10.
549
550 **Fig. S3. Expression of surface receptors in human keratinocytes and**
551 **myoblasts**. Relative transcript levels were determined using quantitative
552 reverse-transcriptase PCR, normalized to the internal *β-actin* standard and
553 relative expression to human myoblasts. All values are means ± standard
554 deviations of four independent experiments. The statistical significance was
555 determined by Student's t test with Welch's correction (*$p<0.05$).
556
557 **Fig. S4. Cytotoxicity of staphylococcal or streptococcal culture**
558 **supernatants on murine myoblasts or human keratinocytes.** Bacterial
559 (NSTI-SA, 6 strains, blue lines; BSI-SA, 3 strains, brown lines; NSTI-GAS, 4
560 strains, green lines) supernatant (1:50 dilution) was added to the cell culture
561 medium containing propidium iodide (PI) and cell death was quantified by
562 monitoring PI incorporation over a 3 hours period. Triton X100 (red line) was
563 used as positive control. Sterile bacterial culture medium (grey line) and cell
564 culture medium (black line) were used as negative controls.
565

bioRxiv preprint doi: https://doi.org/10.1101/530493; this version posted January 28, 2019. The copyright holder for this preprint (which was not certified by peer review) is the author/funder, who has granted bioRxiv a license to display the preprint in perpetuity. It is made available under aCC-BY-NC-ND 4.0 International license.

566 **Fig. S5. Phylogenetic analysis of the *S. aureus* strains.** Rooted phylogenetic
567 analysis using a maximum likelihood approximation based on the 86233 SNPs
568 identified through the conserved core genome of the 30 *S. aureus* strains. The
569 tree is rooted on the clonal complex 1 (MSSA476). NSTI-SA isolates are labeled
570 in red and BSI-SA in black.

571

572 **Text S1.** Detailed genomic analysis of the 30 *S. aureus* strains.

573

bioRxiv preprint doi: https://doi.org/10.1101/530493; this version posted January 28, 2019. The copyright holder for this preprint (which was not certified by peer review) is the author/funder, who has granted bioRxiv a license to display the preprint in perpetuity. It is made available under aCC-BY-NC-ND 4.0 International license.

References

1. Stevens DL, Bryant AE. 2017. Necrotizing Soft-Tissue Infections. N Engl J Med 377:2253–2265.
2. Rajan S. 2012. Skin and soft-tissue infections: classifying and treating a spectrum. Cleve Clin J Med 79:57–66.
3. Miller LG, Rieg G, Bayer AS, Spellberg B. 2005. Necrotizing Fasciitis Caused by Community-Associated Methicillin-Resistant Staphylococcus aureus in Los Angeles. N Engl J Med 9.
4. Chira S, Miller LG. 2010. Staphylococcus aureus is the most common identified cause of cellulitis: a systematic review. Epidemiol Infect 138:313–317.
5. Chiedozi LC. Review of 205 Cases in 112 Patients 5.
6. Christin L, Sarosi GA. 1992. Pyomyositis in North America: Case Reports and Review. Clin Infect Dis 15:668–677.
7. Hall RL, Callaghan JJ, Moloney E, Martinez S, Harrelson JM. 1990. Pyomyositis in a temperate climate. Presentation, diagnosis, and treatment. J Bone Joint Surg Am 72:1240–1244.
8. Hassan FOA, Shannak A. 2008. Primary pyomyositis of the paraspinal muscles: a case report and literature review. Eur Spine J Off Publ Eur Spine Soc Eur Spinal Deform Soc Eur Sect Cerv Spine Res Soc 17 Suppl 2:S239-242.
9. Josse J, Laurent F, Diot A. 2017. Staphylococcal Adhesion and Host Cell Invasion: Fibronectin-Binding and Other Mechanisms. Front Microbiol 8.
10. Szafranska AK, Oxley APA, Chaves-Moreno D, Horst SA, Roßlenbroich S, Peters G, Goldmann O, Rohde M, Sinha B, Pieper DH, Löffler B, Jauregui R, Wos-Oxley ML, Medina E. 2014. High-resolution transcriptomic analysis of the adaptive response of Staphylococcus aureus during acute and chronic phases of osteomyelitis. mBio 5.
11. Rasigade J-P, Trouillet-Assant S, Ferry T, Diep BA, Sapin A, Lhoste Y, Ranfaing J, Badiou C, Benito Y, Bes M, Couzon F, Tigaud S, Lina G, Etienne J, Vandenesch F, Laurent F. 2013. PSMs of Hypervirulent Staphylococcus aureus Act as Intracellular Toxins That Kill Infected Osteoblasts. PLoS ONE 8:e63176.
12. Sinha B, Foti M, Hartford OM, Vaudaux P, Foster TJ, Lew DP, Herrmann M, Krause K-H. 1999. Fibronectin-binding protein acts as Staphylococcus aureus invasin via ®bronectin bridging to integrin a5b. Cell Microbiol 17.
13. Fowler T, Wann ER, Joh D, Johansson S, Foster TJ, Höök M. 2000. Cellular invasion by Staphylococcus aureus involves a fibronectin bridge between the bacterial fibronectin-binding MSCRAMMs and host cell beta1 integrins. Eur J Cell Biol 79:672–679.
14. Selan L, Papa R, Ermocida A, Cellini A, Ettorre E, Vrenna G, Campoccia D, Montanaro L, Arciola CR, Artini M. 2017. Serratiopeptidase reduces the invasion of osteoblasts by *Staphylococcus aureus*. Int J Immunopathol Pharmacol 30:423–428.
15. Trouillet-Assant S, Gallet M, Nauroy P, Rasigade J-P, Flammier S, Parroche P, Marvel J, Ferry T, Vandenesch F, Jurdic P, Laurent F. 2015. Dual Impact of Live Staphylococcus aureus on the Osteoclast Lineage, Leading to Increased Bone Resorption. J Infect Dis 211:571–581.
16. Omland LH, Rasmussen SW, Hvolris J, Friis-Møller A. 2007. Necrotizing fasciitis caused by TSST-1 producing penicillinsensitive Staphylococcus aureus—a case report. Acta Orthop 78:296–297.
17. Morgan WR, Caldwell MD, Brady JM, Stemper ME, Reed KD, Shukla SK. 2007. Necrotizing fasciitis due to a methicillin-sensitive Staphylococcus aureus isolate harboring an enterotoxin gene cluster. J Clin Microbiol 45:668–671.
18. Norrby-Teglund A, Thulin P, Gan BS, Kotb M, McGeer A, Andersson J, Low DE.

bioRxiv preprint doi: https://doi.org/10.1101/530493; this version posted January 28, 2019. The copyright holder for this preprint (which was not certified by peer review) is the author/funder, who has granted bioRxiv a license to display the preprint in perpetuity. It is made available under aCC-BY-NC-ND 4.0 International license.

623 2001. Evidence for superantigen involvement in severe group a streptococcal tissue
624 infections. J Infect Dis 184:853–860.
625 19. Berlon NR, Qi R, Sharma-Kuinkel BK, Joo H-S, Park LP, George D, Thaden JT,
626 Messina JA, Maskarinec SA, Mueller-Premru M, Athan E, Tattevin P, Pericas JM, Woods
627 CW, Otto M, Fowler VG. 2015. Clinical MRSA isolates from skin and soft tissue infections
628 show increased in vitro production of phenol soluble modulins. J Infect 71:447–457.
629 20. Laabei M, Uhlemann A-C, Lowy FD, Austin ED, Yokoyama M, Ouadi K, Feil E,
630 Thorpe HA, Williams B, Perkins M, Peacock SJ, Clarke SR, Dordel J, Holden M, Votintseva
631 AA, Bowden R, Crook DW, Young BC, Wilson DJ, Recker M, Massey RC. 2015.
632 Evolutionary Trade-Offs Underlie the Multi-faceted Virulence of Staphylococcus aureus.
633 PLOS Biol 13:e1002229.
634 21. INFECT Study Group, Siemens N, Kittang BR, Chakrakodi B, Oppegaard O,
635 Johansson L, Bruun T, Mylvaganam H, Arnell P, Hyldegaard O, Nekludov M, Karlsson Y,
636 Svensson M, Skrede S, Norrby-Teglund A. 2015. Increased cytotoxicity and streptolysin O
637 activity in group G streptococcal strains causing invasive tissue infections. Sci Rep 5.
638 22. Rosén A, Arnell P, Madsen MB, Nedrebø BG, Norrby-Teglund A, Hyldegaard O, dos
639 Santos VM, Bergey F, Saccenti E, INFECT Study Group, Skrede S. 2018. Diabetes and
640 necrotizing soft tissue infections-A prospective observational cohort study: Statistical analysis
641 plan. Acta Anaesthesiol Scand 62:1171–1177.
642 23. Bouchiat C, Moreau K, Devillard S, Rasigade J-P, Mosnier A, Geissmann T, Bes M,
643 Tristan A, Lina G, Laurent F, Piroth L, Aissa N, Duval X, Le Moing V, Vandenesch F,
644 French VIRSTA Study Group. 2015. Staphylococcus aureus infective endocarditis versus
645 bacteremia strains: Subtle genetic differences at stake. Infect Genet Evol J Mol Epidemiol
646 Evol Genet Infect Dis 36:524–530.
647 24. Fey PD, Endres JL, Yajjala VK, Widhelm TJ, Boissy RJ, Bose JL, Bayles KW. 2013.
648 A genetic resource for rapid and comprehensive phenotype screening of nonessential
649 Staphylococcus aureus genes. mBio 4:e00537-00512.
650 25. Bae T, Schneewind O. 2006. Allelic replacement in Staphylococcus aureus with
651 inducible counter-selection. Plasmid 55:58–63.
652 26. Diep BA, Chan L, Tattevin P, Kajikawa O, Martin TR, Basuino L, Mai TT, Marbach
653 H, Braughton KR, Whitney AR, Gardner DJ, Fan X, Tseng CW, Liu GY, Badiou C, Etienne
654 J, Lina G, Matthay MA, DeLeo FR, Chambers HF. 2010. Polymorphonuclear leukocytes
655 mediate Staphylococcus aureus Panton-Valentine leukocidin-induced lung inflammation and
656 injury. Proc Natl Acad Sci U S A 107:5587–5592.
657 27. Dickson MA, Hahn WC, Ino Y, Ronfard V, Wu JY, Weinberg RA, Louis DN, Li FP,
658 Rheinwald JG. 2000. Human Keratinocytes That Express hTERT and Also Bypass a
659 p16INK4a-Enforced Mechanism That Limits Life Span Become Immortal yet Retain Normal
660 Growth and Differentiation Characteristics. Mol Cell Biol 20:1436–1447.
661 28. Yaffe D, Saxel O. 1977. Serial passaging and differentiation of myogenic cells
662 isolated from dystrophic mouse muscle. Nature 270:725–727.
663 29. Bigot A, Duddy WJ, Ouandaogo ZG, Negroni E, Mariot V, Ghimbovschi S, Harmon
664 B, Wielgosik A, Loiseau C, Devaney J, Dumonceaux J, Butler-Browne G, Mouly V, Duguez
665 S. 2015. Age-Associated Methylation Suppresses SPRY1, Leading to a Failure of Re-
666 quiescence and Loss of the Reserve Stem Cell Pool in Elderly Muscle. Cell Rep 13:1172–
667 1182.
668 30. Vilette D, Laulagnier K, Huor A, Alais S, Simoes S, Maryse R, Provansal M,
669 Lehmann S, Andreoletti O, Schaeffer L, Raposo G, Leblanc P. 2015. Efficient inhibition of
670 infectious prions multiplication and release by targeting the exosomal pathway. Cell Mol Life
671 Sci CMLS 72:4409–4427.
672 31. Alais S, Soto-Rifo R, Balter V, Gruffat H, Manet E, Schaeffer L, Darlix JL, Cimarelli

bioRxiv preprint doi: https://doi.org/10.1101/530493; this version posted January 28, 2019. The copyright holder for this preprint (which was not certified by peer review) is the author/funder, who has granted bioRxiv a license to display the preprint in perpetuity. It is made available under aCC-BY-NC-ND 4.0 International license.

673 A, Raposo G, Ohlmann T, Leblanc P. 2012. Functional mechanisms of the cellular prion
674 protein (PrPC) associated anti-HIV-1 properties. Cell Mol Life Sci 69:1331–1352.
675 32. Thorley M, Duguez S, Mazza EMC, Valsoni S, Bigot A, Mamchaoui K, Harmon B,
676 Voit T, Mouly V, Duddy W. 2016. Skeletal muscle characteristics are preserved in
677 hTERT/cdk4 human myogenic cell lines. Skelet Muscle 6.
678 33. Trouillet S, Rasigade J-P, Lhoste Y, Ferry T, Vandenesch F, Etienne J, Laurent F.
679 2011. A novel flow cytometry-based assay for the quantification of Staphylococcus aureus
680 adhesion to and invasion of eukaryotic cells. J Microbiol Methods 86:145–149.
681

TABLE 1 Quantification of intracellular bacteria assessed by transmission electron microscopy

Cells	Strains	Number of analysed cells	Number of infected cells[a]	Number of bacteria in infected cells[a]	Mean number of bacteria per infected cells	Percentage of infected cells
Myoblasts	INFECT2127	301	44	154	3,5	14.62
	SF8300	175	20	76	3.8	11.43
Keratinocytes	INFECT2127	455	13	45	3.46	2.86
	SF8300	491	7	26	3.7	1.43

[a]Assessed by visual counting of TEM sections

bioRxiv preprint doi: https://doi.org/10.1101/530493; this version posted January 28, 2019. The copyright holder for this preprint (which was not certified by peer review) is the author/funder, who has granted bioRxiv a license to display the preprint in perpetuity. It is made available under aCC-BY-NC-ND 4.0 International license.

TABLE 2 Frequency of the genes detected by DNA microarray in *S. aureus* NSTI and BSI isolates[a].

bioRxiv preprint doi: https://doi.org/10.1101/530493; this version posted January 28, 2019. The copyright holder for this preprint (which was not certified by peer review) is the author/funder, who has granted bioRxiv a license to display the preprint in perpetuity. It is made available under aCC-BY-NC-ND 4.0 International license.

Gene or allele	NSTI isolates (%) n = 9	BSI isolates (%) n = 21	P adjust[b]
Adhesins encoding genes			
fnbA	9 (100)	21 (100)	1.000
fnbB	6 (66.7)	19 (90.5)	1.000
clfA	9 (100)	21 (100)	1.000
clfB	9 (100)	21 (100)	1.000
cna	5 (55.6)	8 (38.1)	1.000
spa	9 (100)	21 (100)	1.000
sdrC	9 (100)	21 (100)	1.000
sdrD	7 (77.8)	20 (95.2)	1.000
bbp	5 (55.6)	21 (100)	0.156
ebpS	9 (100)	21 (100)	1.000
map/eap	7 (77.8)	20 (95.2)	1.000
Toxins encoding genes			
eta	0 (0)	1 (4.8)	1.000
etb	0 (0)	0 (0)	1.000
tst1	2 (22.2)	3 (14.3)	1.000
sea	1 (11.1)	2 (9.5)	1.000
seb	2 (22.2)	0 (0)	1.000
sec	1 (11.1)	2 (9.5)	1.000
sed	0 (0)	5 (23.8)	1.000
see	0 (0)	0 (0)	1.000
seg	5 (55.6)	15 (71.4)	1.000
seh	1 (11.1)	0 (0)	1.000
sei	5 (55.6)	15 (71.4)	1.000
sej	0 (0)	5 (23.8)	1.000
Superantigen[c]	7 (77.8)	18 (85.7)	1.000
*luk*S-PV	1 (11.1)	0 (0)	1.000
hla	9 (100)	21 (100)	1.000
hlb[123] (d)	7 (77.8)	18 (85.7)	1.000
func_hlb (e)	0 (0)	0 (0)	1.000
Other putative virulence factors encoding genes			

bioRxiv preprint doi: https://doi.org/10.1101/530493; this version posted January 28, 2019. The copyright holder for this preprint (which was not certified by peer review) is the author/funder, who has granted bioRxiv a license to display the preprint in perpetuity. It is made available under aCC-BY-NC-ND 4.0 International license.

icaA	9 (100)	21 (100)	1.000
chp	8 (88.9)	15 (71.4)	1.000
Regulation encoding genes			
agrI	6 (66.7)	7 (33.3)	1.000
agrII	1 (11.1)	10 (47.6)	1.000
agrIII	2 (22.2)	2 (9.5)	1.000
agrIV	0 (0)	2 (9.5)	1.000

[a]NSTI, Necrotizing Soft Tissue Infection; BSI, BloodStream Infection; [b]P-values are calculated for each gene or allele with a two-tailed Fisher's exact test. Bonferronni correction was applied; [c]At least one superantigen; [d]hlb123 represents *hlb* encoding gene alleles detected by one of the probes 1,2,3; [e]func_hlb accounts for the *hlb* functional encoding gene.

bioRxiv preprint doi: https://doi.org/10.1101/530493; this version posted January 28, 2019. The copyright holder for this preprint (which was not certified by peer review) is the author/funder, who has granted bioRxiv a license to display the preprint in perpetuity. It is made available under aCC-BY-NC-ND 4.0 International license.

TABLE 3 Description of clinical strains used in this study[a]

bioRxiv preprint doi: https://doi.org/10.1101/530493; this version posted January 28, 2019. The copyright holder for this preprint (which was not certified by peer review) is the author/funder, who has granted bioRxiv a license to display the preprint in perpetuity. It is made available under aCC-BY-NC-ND 4.0 International license.

Species	Disease category	Clinical diagnosis	Site of isolation	Strain n°	CC or emm type	Source (ref)
S. ***aureus***	Invasive	NSTI	Fascia	ST2014**1878**	CC188	NRCS (this study)
	Invasive	NSTI	Fascia	ST2014**0479**	CC8	NRCS (this study)
	Invasive	NSTI	Fascia	ST2014**0899**	CC45	NRCS (this study)
	Invasive	NSTI	Fascia	ST2014**1963**	CC30	NRCS (this study)
	Invasive	Extensive cellulitis	Blood	ST2015**1186**	CC25	NRCS (this study)
	Invasive	NSTI	Subcutaneous tissue	INFECT**2023/**ST2017**0477**	CC30	INFECT (this study)
	Invasive	NSTI	Subcutaneous tissue	INFECT**2127/**ST2017**0479**	CC15	INFECT (this study)
	Invasive	NSTI	Subcutaneous tissue	INFECT**3045/**ST2017**0482**	CC188	INFECT (this study)
	Invasive	NSTI	Blood	INFECT**6005/**ST2014**0625**	CC45	INFECT (this study)
	Invasive	Endocarditis	Blood	ST2011**1452**	CC5	(1)
	Invasive	Endocarditis	Blood	ST2010**2292**	CC5	(1)
	Invasive	Endocarditis	Blood	ST2010**1433**	CC97	(1)
	Invasive	Endocarditis	Blood	ST2009**1672**	CC8	(1)
	Invasive	Endocarditis	Blood	ST2009**1693**	CC45	(1)
	Invasive	Endocarditis	Blood	ST2009**1729**	CC22	(1)
	Invasive	Endocarditis	Blood	ST2010**0860**	CC30	(1)
	Invasive	Endocarditis	Blood	ST2010**2139**	CC398	(1)
	Invasive	Endocarditis	Blood	ST2010**2295**	CC5	(1)
	Invasive	Endocarditis	Blood	ST2011**0560**	CC5	(1)
	Invasive	Endocarditis	Blood	ST2011**1220**	CC121	(1)
	Invasive	Endocarditis	Blood	ST2011**1368**	CC15	(1)
	Invasive	Bacteremia	Blood	ST2009**1950**	CC8	(1)
	Invasive	Bacteremia	Blood	ST2009**1954**	CC30	(1)
	Invasive	Bacteremia	Blood	ST2010**1786**	CC45	(1)
	Invasive	Bacteremia	Blood	ST2010**1791**	CC5	(1)
	Invasive	Bacteremia	Blood	ST2010**2304**	CC121	(1)
	Invasive	Bacteremia	Blood	ST2011**0552**	CC15	(1)
	Invasive	Bacteremia	Blood	ST2011**1372**	CC5	(1)
	Invasive	Bacteremia	Blood	ST2012**0206**	CC5	(1)
	Invasive	Bacteremia	Blood	ST2012**0211**	CC5	(1)
S. ***pyogenes***	Invasive	NSTI	Blood	INFECT**2006**	emm1	(2)
	Invasive	NSTI	Tissue	INFECT**2028**	emm3	(2)
	Invasive	NSTI	Wound	INFECT**5004**	emm28	(2)
	Invasive	NSTI	Wound Tissue	INFECT**5006**	emm1	(2)
S. ***epidermidis***	Non invasive	Nose colonization	Nose	CCM2124		
S. ***haemolyticus***	Non invasive	ND	Skin	CCM2737		
S. ***hominis***	Non invasive	ND	Skin	DSM20328		
S. ***lugdunensis***	Non invasive	Breast abscess	Axillary node	ATCC43809		
S. ***saprophyticus***	Non invasive	UTI	Urine	CCM883		
S. ***warneri***	Non invasive	ND	Skin	CCM2730		

[a]NSTI, Necrotizing Soft Tissue Infection; CC, Clonal Complex; emm, M protein gene; UTI, Urinary Tract Infection; ND, Not Determine

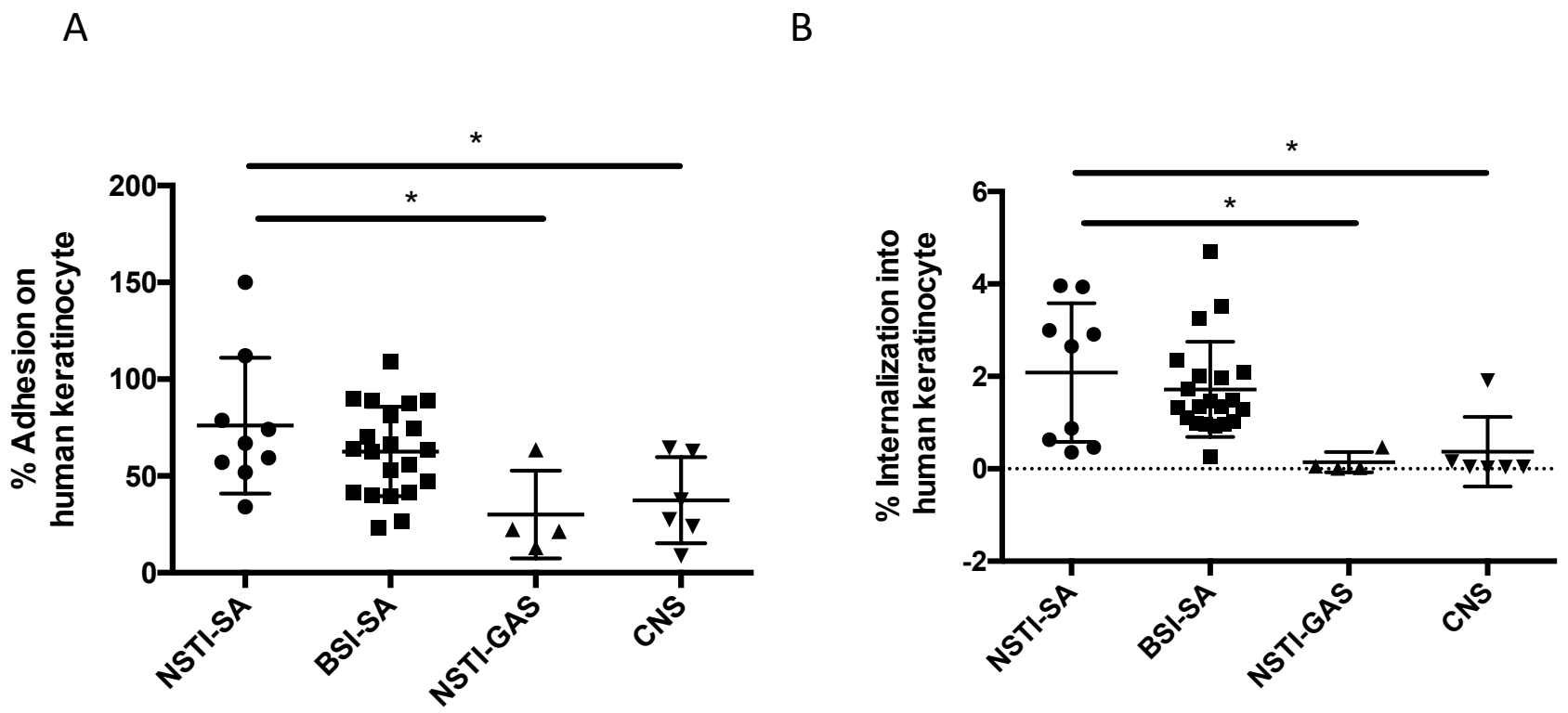

Fig.1

Fig. 1. Adhesion and internalization of *Staphylococcus aureus* (SA), coagulase negative *Staphylococcus* (CNS) and group A *Streptococcus* (GAS) to human keratinocytes. (A) Percentages of adhered bacteria were calculated after 2 hours of infection in relation to inoculum of infection. Intracellular bacteria assessed in B were subtracted; (B) Internalization was determined after 2 hours of infection followed by antibiotic treatment to exclude extracellular bacteria. Multiplicity of infection (MOI) = 10. The horizontal lines within each group represent the mean value ± standard deviations of at least three independent experiments per strain. *p<0.05, **p<0.01, *** p<0.001.

Fig. 2. Adhesion and internalization of *Staphylococcus aureus* (SA), coagulase negative *Staphylococcus* (CNS) and group A *Streptococcus* (GAS) to murine and human myoblasts. (A and B) Percentages of adherent bacteria were calculated after 2 hours of infection in relation to inoculum of infection. Intracellular bacteria assessed in C and D were subtracted; (C and D) Internalization was determined after 2 hours of infection followed by antibiotic treatment to exclude extracellular bacteria. Multiplicity of infection (MOI) = 10. The horizontal lines within each group represent the mean value ± standard deviations of at least three independent experiments per strain. *p<0.05, **p<0.01, *** p<0.001, ****p<0,0001.

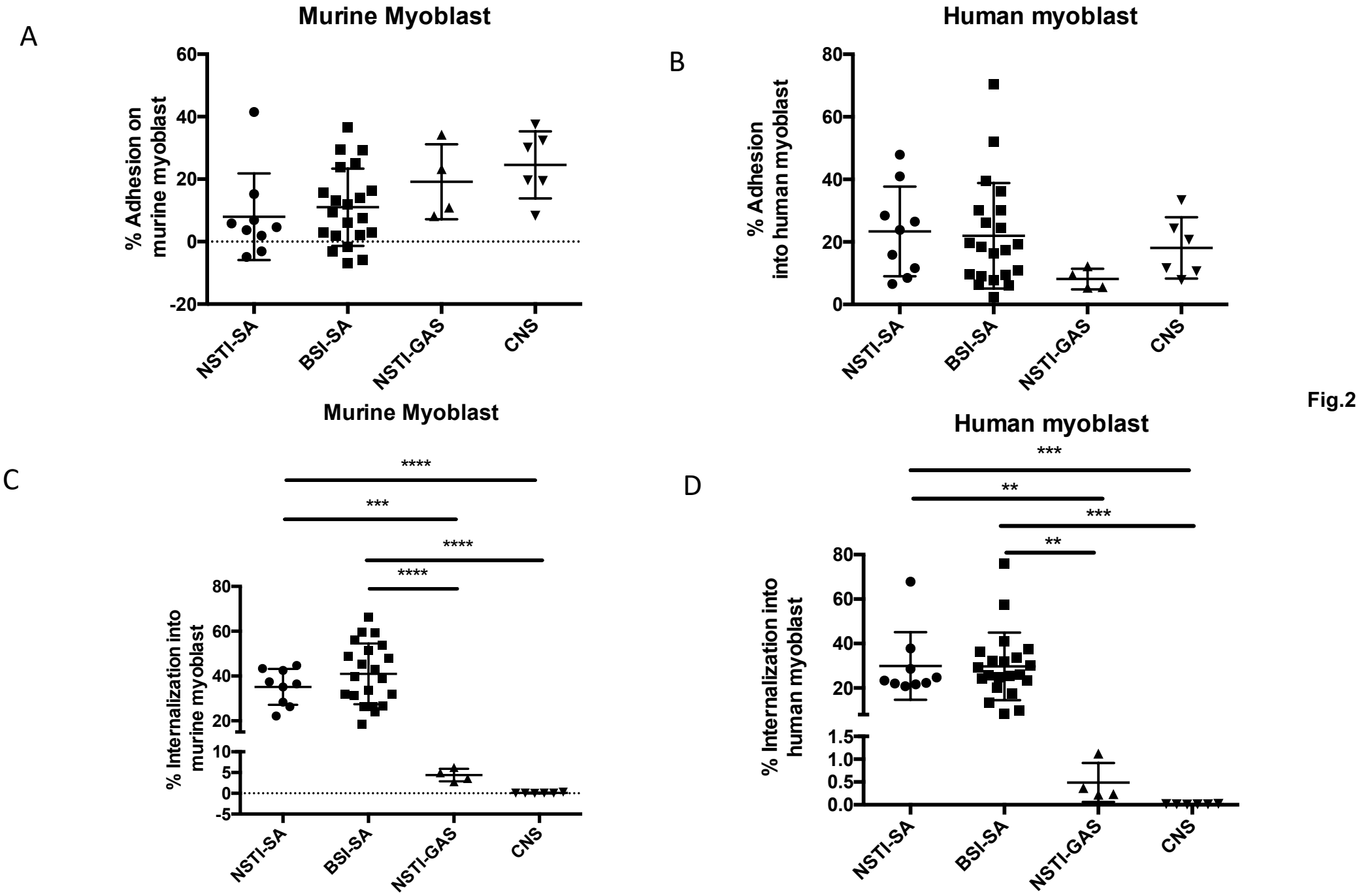

Fig.2

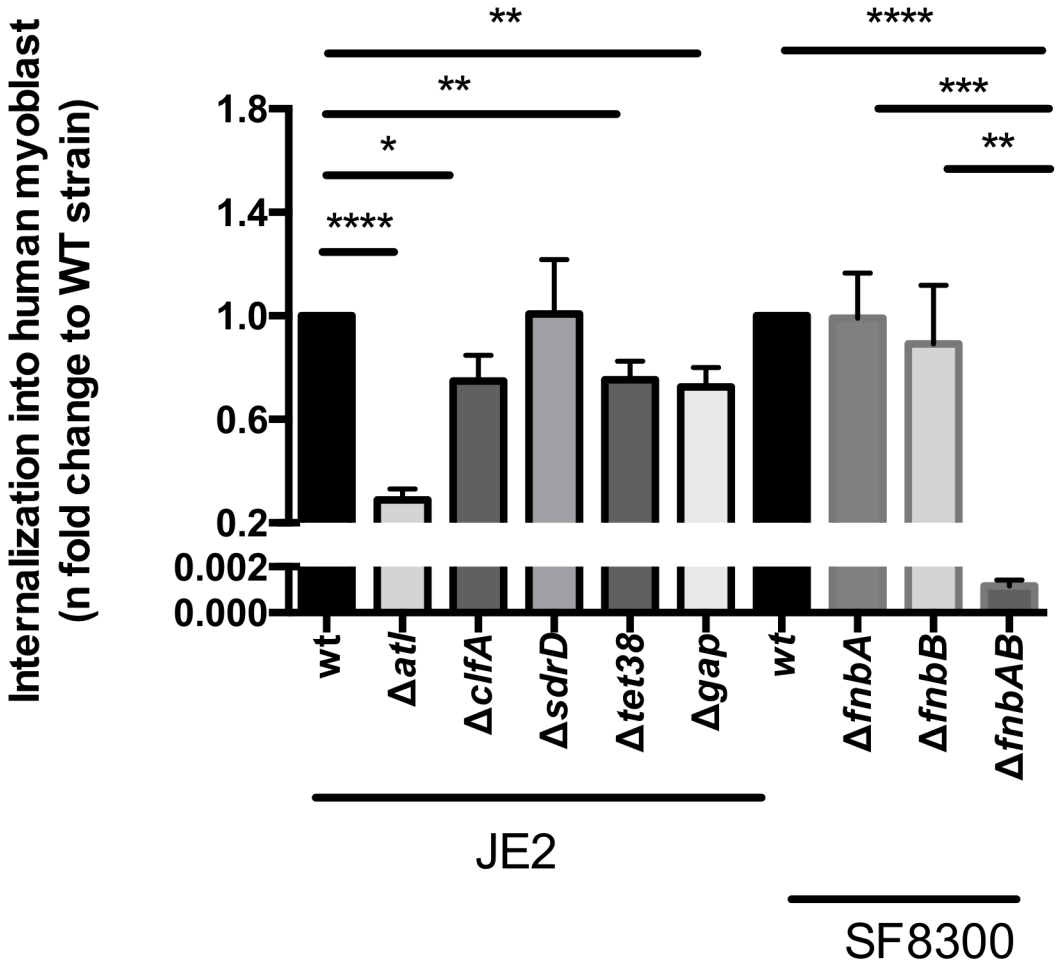

Fig. 3. Internalization of *S. aureus* mutants into human myoblasts. Internalization of the various mutants in genes encoding surface proteins was determined after 2 hours of infection followed by antibiotic treatment to exclude extracellular bacteria. The internalization was normalized to that of wild type strain. Multiplicity of infection (MOI) = 10. All values are means ± standard error of mean of three independents experiments in duplicate for each strain. *p<0.05, **p<0.01, *** p<0.001, ****p<0,0001.

Fig.3

A

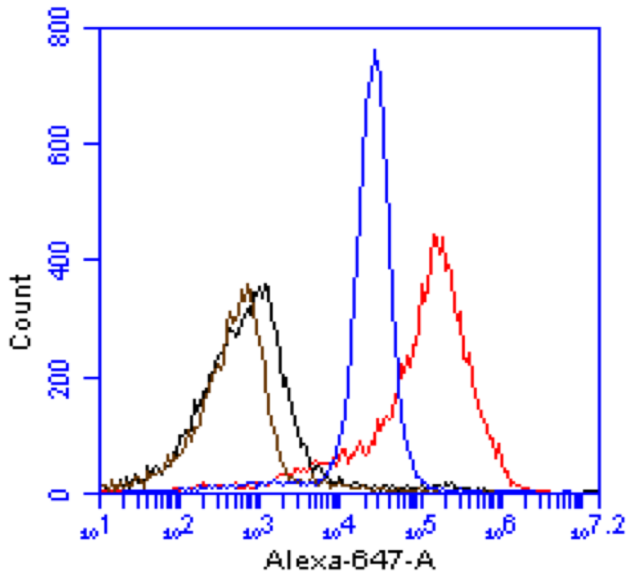

			MFI
Human myoblast		IgG control	7762
		Ac anti-α5β1	244368

			MFI
Human keratinocyte		IgG control	983
		Ac anti-α5β1	30011

B

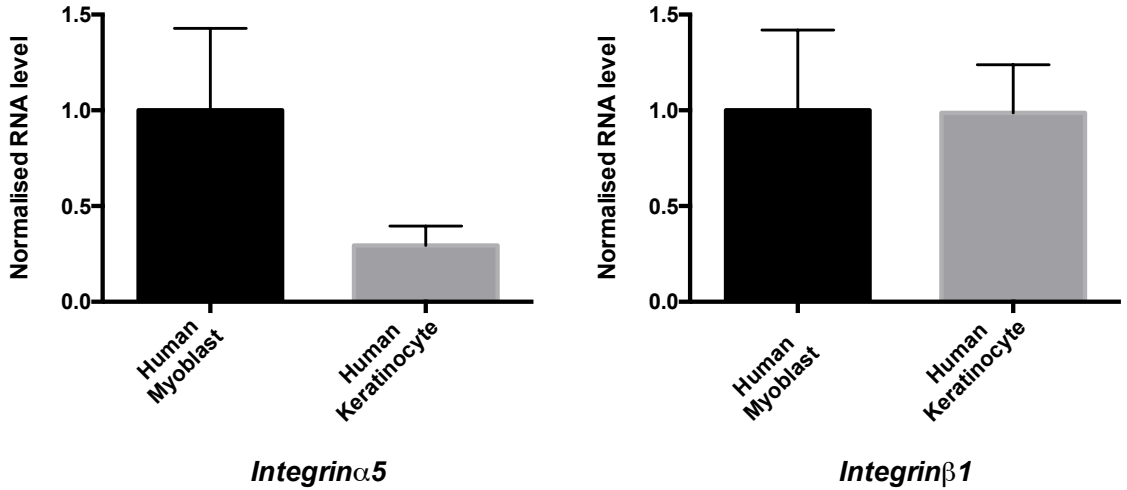

Fig.4

Fig. 4. Expression of α5β1 integrin by human keratinocyte and myoblasts. (A) Cell surface expression of α5β1 integrin assessed by flow cytometry and α5β1 antibody**;** (B) Relative transcript levels of α5, β1 integrin sub-units were determined using quantitative reverse-transcriptase PCR, normalized to the internal *β-actin* standard. All values are means ± standard error of mean of four independents experiments.

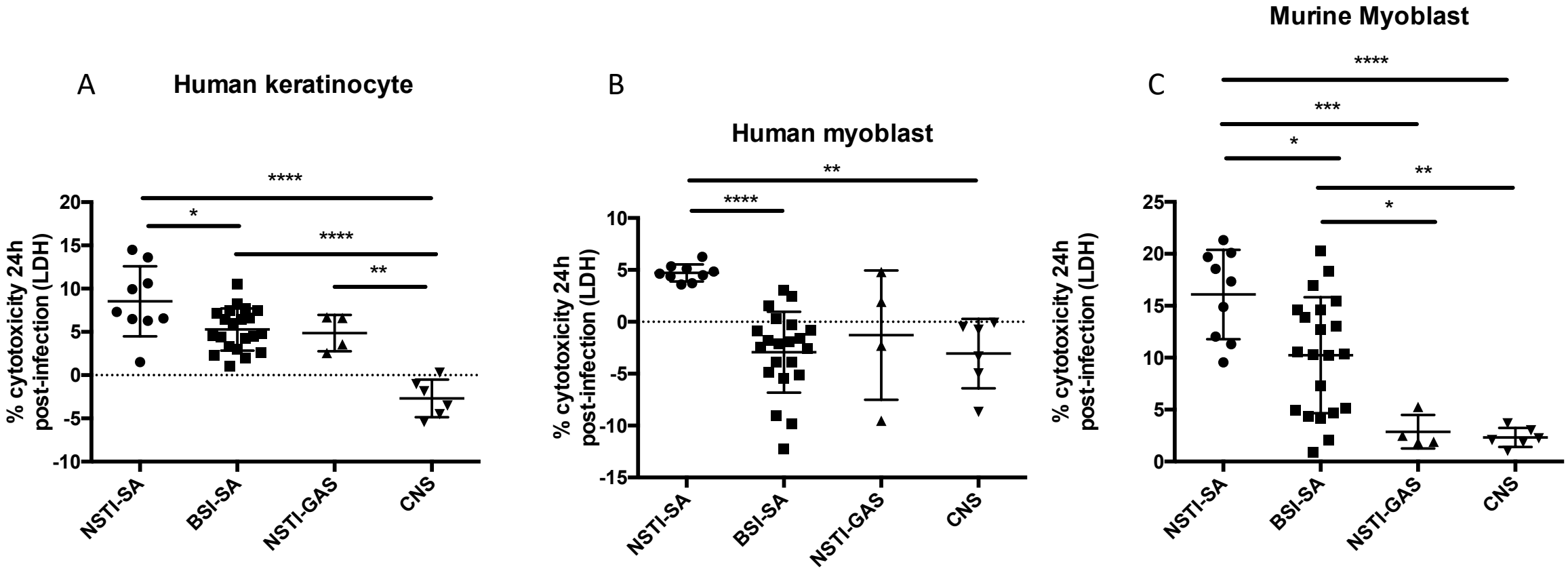

Fig.5

Fig. 5. Cytotoxicity of intracellular bacteria at 24h post infection. Cytotoxicity was estimated by quantifying LDH release by infected cells at 24 hours post infection. Multiplicity of infection (MOI) = 10. The percentage of cytotoxicity was calculated as follows: ((LDH infected cells - LDH lower control)/(LDH higher control - LDH lower control)) x100. The horizontal lines within each group represent the mean value ± standard deviations of at least three independent experiments per strain. *p<0.05, **p<0.01, *** p<0.001, ****p<0,0001.

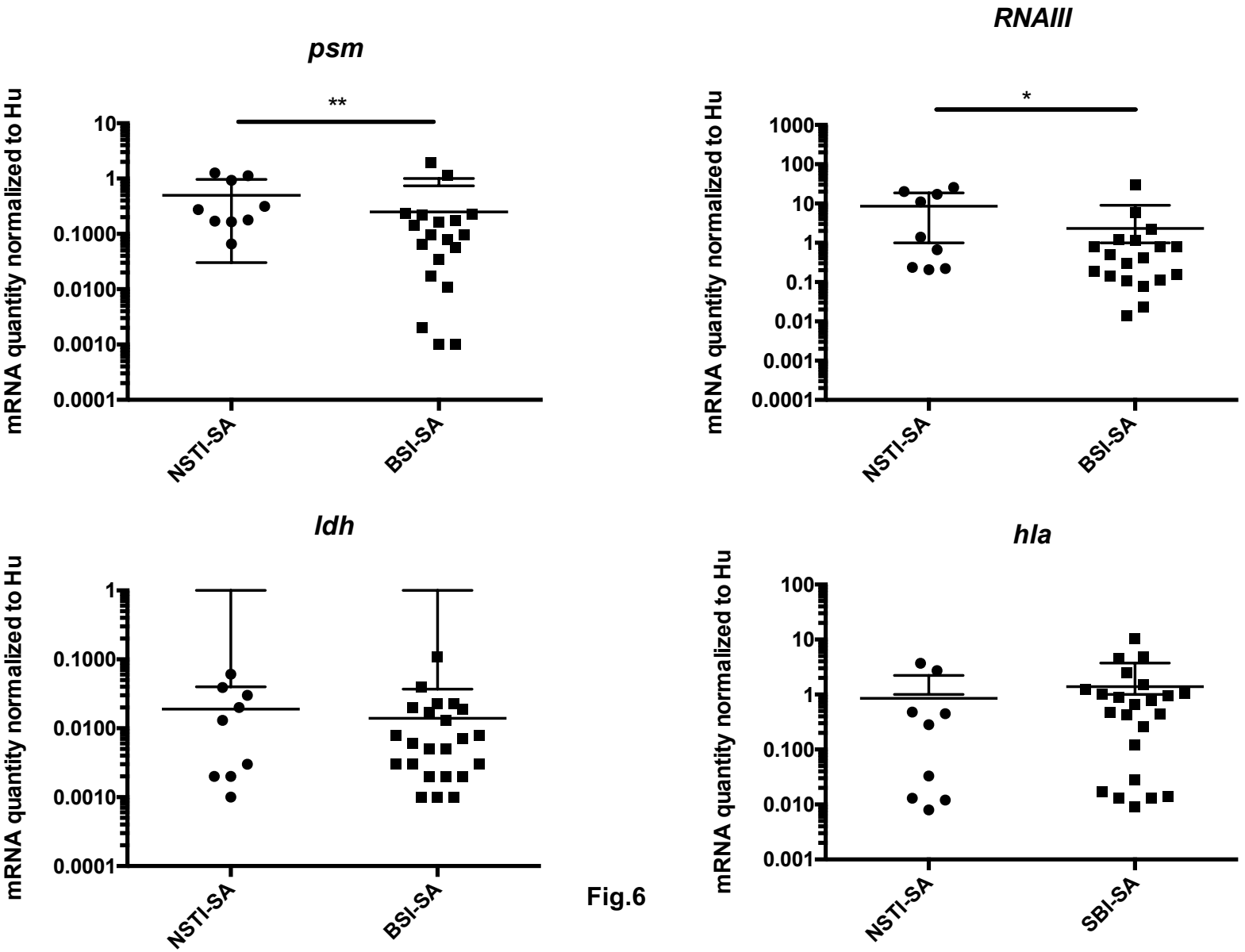

Fig. 6. Expression of intracellular bacterial mRNA into human myoblasts 3 hours post infection. Relative transcript levels were determined using quantitative reverse-transcriptase PCR and expressed as n-fold change to the internal *hu* standard. The horizontal lines within each group represent the mean value ± standard deviations. *p<0.05, **p<0.01.

Fig.6